DYNAMIC DELAMINATION OF AERONAUTIC STRUCTURAL COMPOSITES BY USING COHESIVE FINITE ELEMENTS

M. Ilyas, F. Lachaud[1], Ch. Espinosa and M. Salaün
Université de Toulouse, ISAE/DMSM,
10 avenue Edouard Belin, 31400 Toulouse
frederic.lachaud@isae.fr

SUMMARY

Cohesive finite elements are used to model impact induced delamination prediction of T800/21M unidirectional laminated composite. DCB, ELS and MMB tests are used to identify cohesive element parameters. Results from experiments and numerical prediction of impact induced delamination by commercially available code LS-DYNA are compared.

Keywords: impact, cohesive elements, carbon/epoxy composites, rapid dynamics.

INTRODUCTION

Aircraft secondary structures have been manufactured by composite materials for a long time. The ability to use these materials in primary structures requires the designers to understand damage initiation and propagation phenomena strongly influencing residual strength and therefore certification process. In order to achieve this aim calculations and experiments are conducted. The mechanical behavior of laminates is often represented by finite element method (FEM). It is common to integrate damage initiation and propagation laws in constitutive equations. Some of the methods of impact induced delamination prediction by FEM are reviewed in ref [1]. We have chosen the cohesive finite element approach presented by Camanho et al [2], which was first used in an implicit finite element code, and, later on, in an explicit finite element code by Iannucci [3] and Pinho et al [4]. This material model distinguishes two constants (i) damage initiation threshold, and (ii) critical release energy rate for relative delamination propagation mode. Our interest has been in the use of arising numerical methods to model these damage related openings, with special focus on the residual strength prediction for a wide range of impact loadings. The present work is devoted to cohesive finite element parameter identification. In the first part of the paper we present the cohesive finite element material model and cohesive element parameter calibration based in mode I, mode II and mixed mode critical energy release rates measured by DCB, ELS and MMB tests. In the second part we apply these findings to an aeronautical composite plate made of T800/M21 unidirectional carbon fiber and epoxy plies as a first but not easiest modeling step to predict medium range velocity impact behavior. A 10J impact case is chosen to compare numerical and experimental results.

[1] Corresponding author

Other parts of the present work dealing with use of meshless numerical methods can be found in ref [5].

COHESIVE ELEMENT PARAMETER IDENTIFICATION

Material model for cohesive elements

The developed model based on traction separation law is very similar to a material model already available in LS-DYNA [6]. The mixed-mode displacement generating rupture in a cohesive element is given by:

$$\delta_r = \frac{2(1+\beta)^2}{\delta_0}\left[\left(\frac{k_n}{G_{Ic}}\right)^{\alpha} + \left(\frac{k_s\beta^2}{G_{IIc}}\right)^{\alpha}\right]^{\frac{-1}{\alpha}} \tag{1}$$

$$\delta_0 = \delta_{I_0}\delta_{II_0}\sqrt{\frac{1+\beta^2}{\left(\delta_{II_0}\right)^2 + \left(\beta\delta_{I_0}\right)^2}} \qquad \beta = \frac{\delta_{II}}{\delta_I} \qquad \delta_{I_0} = \frac{\sigma_n}{k_n} \qquad \delta_{II_0} = \frac{\sigma_s}{k_s} \tag{2}$$

The model was implemented in LS-DYNA via a user defined cohesive material subroutine with an aim to add strain rate effects at a later stage. It is evident from equation 2 that mixed mode damage initiation displacement (δ_0), softening threshold, tends towards pure mode I when β approaches zero, i.e. when the displacement components of the cohesive element are zero except the local opening (z-component). In a pure mode II scenario, i.e. when local z-component is zero, a large value (1×10^{20}) of β is chosen to avoid division by zero and δ_0 and δ_r are set equal to δ_{II_0} and δ_{II_m} respectively.

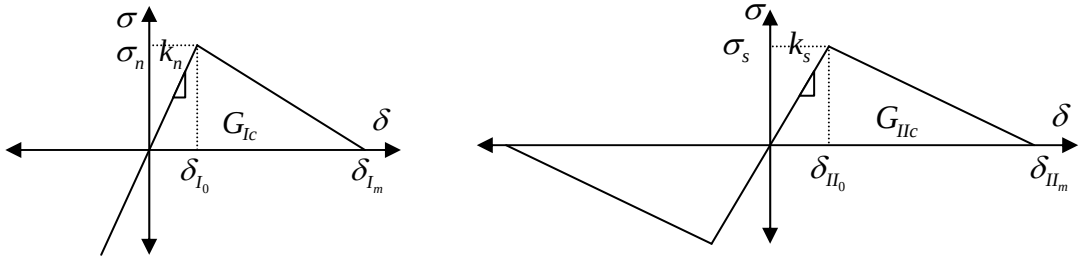

Figure 1: Cohesive material model, pure mode I (LHS), and pure mode II (RHS).

Further details of mixed mode model can be found in ref [4] and [6].

Numerical data identification from experimental results

In the following paragraphs we shall discuss numerical and experimental results of (i) double cantilever beam (DCB), (ii) end load split (ELS) and (iii) mixed mode bending (MMB) test. The finite element models consist of under integrated (1 integration point) 8 node brick elements with 1 element across thickness for composite arms. A zero thickness layer of 4 point cohesive elements is placed between the two composite arms. Cohesive elements are killed once the δ_r is attained at any one integration point. Loading and boundary conditions are explained in corresponding paragraphs.

Mode I:

Double cantilever beam (DCB) tests of T800/M21 were conducted with specimen dimensions as 120 *mm* (L) × 25 *mm* (b) × 3.1 *mm* (2h). A pre-crack (a_0) of 40 *mm* is realized by introducing a 13 *μm* thick Teflon film. Tests were carried out on a servo-hydraulic machine under a constant displacement rate of 2 *mm/min* for quasi-static [8] and 30 *m/min* (0.5 *m/sec*) for pseudo-dynamic tests. For dynamic tests the specimen is pre-cracked up to 45 (±1) *mm* to avoid artificial increase in critical strain energy release rate values often observed in the case of mode II [9]. The composite material has an isotropic material with flexural modulus of 120 *GPa*, normal and tangential stiffness were 100 kN/mm^3, normal and tangential failure stresses were 60 *MPa*. Mode I critical energy release rate is 765 J/m^2. Composite arms opening rate of 0.5 *m/sec* was applied as a constant nodal velocity (see Figure 1 RHS). To prevent hourglass mode perpendicular to *xz*-plane, translations in *y* are blocked.

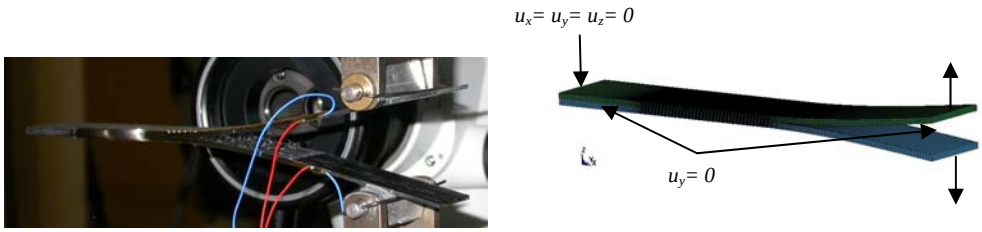

Figure 2: DCB experimental setup (LHS), and numerical model (RHS).

For quasi static and dynamic tests there was no considerable difference in overall form of the force displacement curve, as shown in Figure 3, thus it can be said that the strain rate effects are not apparent in this range of loading speeds. In future it is envisaged to conduct tests at higher strain rates by using split Hopkinson's pressure bar.

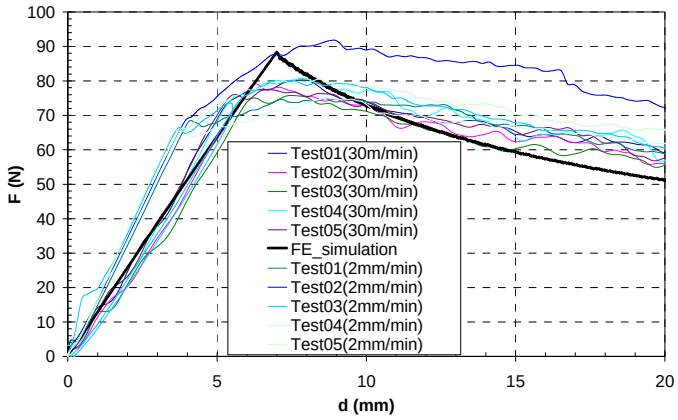

Figure 3: Force displacement curves: numerical and experimental results (T800/M21).

It can be seen in Figure 3 that results of numerical simulation and experimental force displacement curves are in close comparison. Slightly higher values of peak force and corresponding displacement on numerical curve can be attributed to a bit too stiff mode I numerical model. Details of experimental results can be found in ref [7].

Mode II:

Experimental results of quasi-static end load split (ELS) tests for pure mode II of T700/M21 are taken from ref [89]. Specimen dimensions are 140 *mm* (L) × 20 *mm* (b) × 4.68 *mm* (2h). A pre-crack (a_0) of 80 *mm* is introduced by a 13 μm thick Teflon film. This crack is propagated by 4 *mm* in order to break the resin present near the end of Teflon film. Hence numerical model has a pre-crack of 84 *mm*. Orthotropic elastic material constants are shown in Table 1. Cohesive element properties are same as for mode I simulations. Mode II fracture toughness (G_{IIc}) value used for numerical simulation is 1387 J/m^2.

Table 1: Material properties used for ELS and MMB simulations of T700/M21.

E_{11f}	E_{22}	E_{33}	ν_{12}	ν_{23}	ν_{13}	G_{12}	G_{23}	G_{13}
98.62 *GPa*	7.69 *GPa*	7.69 *GPa*	0.33	0.33	0.40	4.75 *GPa*	2.75 *GPa*	4.75 GPa

In experimental setup, load cell is allowed to move only vertical to the plane of specimen; lateral displacement of specimen is allowed by using a moveable support as shown in Figure 4 (LHS). In the simplified numerical model we have fixed the left side while right end is free to move in x-direction as a consequence of applied displacement (240 *mm/sec*) in positive z-direction.

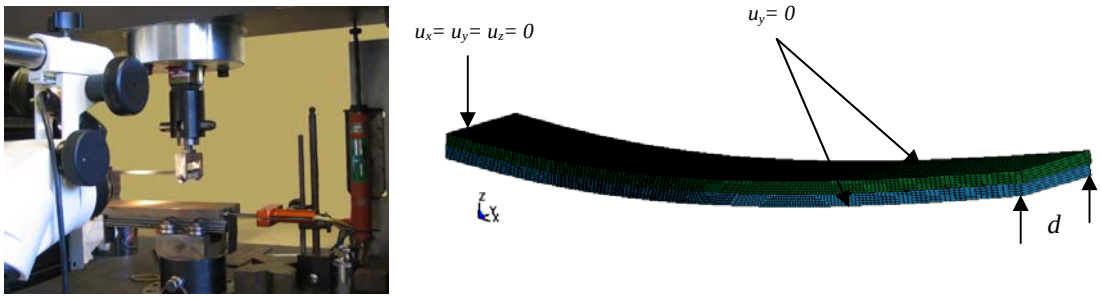

Figure 4: ELS experimental setup (LHS), and numerical model (RHS).

Comparison of experiments and numerical simulations reveals a small difference (less than 10 %) in peak force and beam end displacement. This mismatch can be attributed to the dissimilarity of boundary conditions for experimental and finite element results.

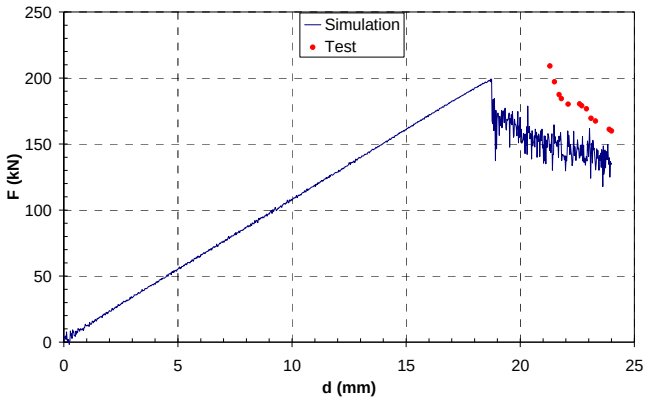

Figure 5: Comparison of experimental results (T700/M21) and numerical simulation for ELS specimen.

Mixed mode:

In order to test the validity of numerical model in a mixed mode loading, we simulate mixed mode bending (MMB) test of T700/M21, with 50 % mode I, from ref [9]. Specimen dimensions are 100 *mm* (2L) × 20 *mm* (b) × 4.68 *mm* (2h). A pre-crack (a_0) of 25 *mm* is introduced in a similar method as described above for ELS and DCB. For numerical simulations the pre-crack is 29 *mm*, the value obtained by a small pre-cracking as is done for pure mode I and mode II tests. A somewhat complicated mounting and loading fixture is modeled by using rigid elements and joints. Material properties for composite arms are same as reported earlier in Table 1. Average values of G_{Ic} and G_{IIc} are 545 J/m^2 and 1387 J/m^2 respectively. The constant α defining mixed mode delamination propagation (Eq 2) is 1.5.

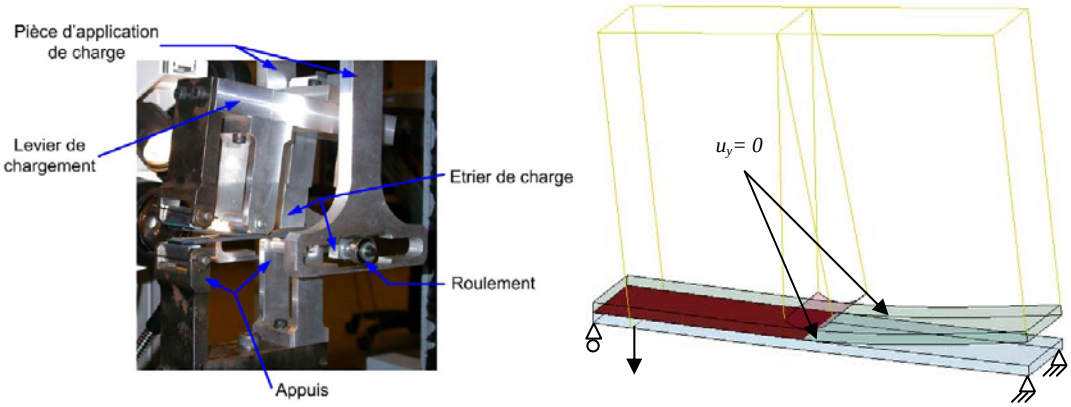

Figure 6: MMB experimental setup (LHS), and numerical model (RHS).

Results from numerical simulation and tests are traced in Figure 7. Numerical model is in close agreement with experimental results for both force and displacement.

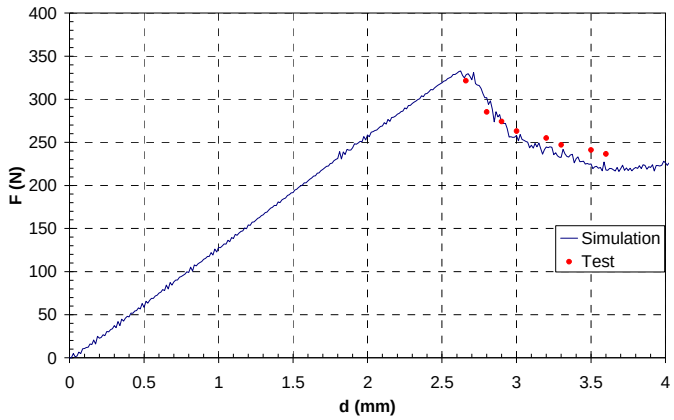

Figure 7: Comparison numerical simulation and experimental results.

APPLICATION TO IMPACT DAMAGE MODELING

Several impact models with T800/M21 material properties have been tested to evaluate the ability of numerical model to predict different combinations of damage modes. Results chosen are for a stratification that is used in aeronautical parts in order to reduce the extent of delamination in the interfaces next to external plies. Damages are confined in a more cylindrical through thickness zone around the impact point, instead of the

"well known" helicoidally conical shape, essentially due to the position of the [45/-45] interface. The 150 *mm* × 75 *mm* × 2.5 *mm* plate is simply supported on a thick metallic plate with a rectangular opening of 125 *mm* × 75 *mm*. It is impacted by a rigid hemisphere of radius 8 *mm* and velocity 2.955 *m/s* (about 10.3 *J*) using a classical drop weight impact setup. Experimental and numerical results are the maximum force vs time and displacement vs time curves. C-Scan measurements for delamination estimation are compared to damage extent reported by simulation.

Table 2: Material properties for used for simulations of T800/M21.

E_{11}	E_{22}	E_{33}	ν_{12}	ν_{23}	ν_{13}	G_{12}	G_{23}	G_{13}
157 *GPa*	8.5 *GPa*	8.5 *GPa*	0.35	0.35	0.53	4.2 *GPa*	2.2 *GPa*	4.2 *GPa*
k_n	k_s	σ_n	σ_s	G_{Ic}	G_{IIc}	α		
100 N/mm^3	100 N/mm^3	60 *MPa*	60 *MPa*	765 J/m^2	1250 J/m^2	1.0		

A single eight node brick element with 3 DOF per node and 1 integration point has been used in thickness direction for the plies. Frictionless contact algorithms are defined between (i) plate and support, (ii) plate and hemisphere, (iii) ply interfaces to treat post cohesive element failure behavior. Material properties for composite plies and cohesive elements are presented in Table 2. For [45/-45] interfaces a lower value of maximum tangential stress, 40 *MPa*, is chosen. The impact model, layering, and cohesive zones are presented in Figure 8.

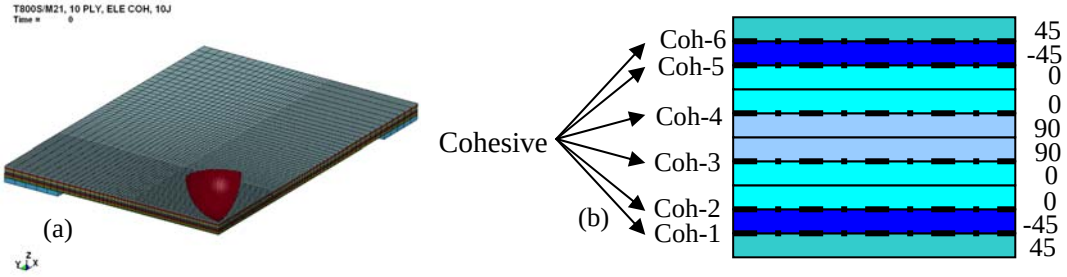

Figure 8: (a) ¼ view of 3D numerical model (b) and cohesive element location and labels.

Adding the cohesive elements between the plies in the FE elastic model doesn't change the global shape of the curves, neither the loading slopes, but the peak values and the time duration of the contact with the projectile show loss of stiffness during the loading phase of the impact. Compared to the experimental force curve, the cohesive model is too stiff. Surely this discrepancy is due to the lack of damage in the model. To quantify the inaccuracy part of the cohesive model, delaminated areas are compared with C-scan.

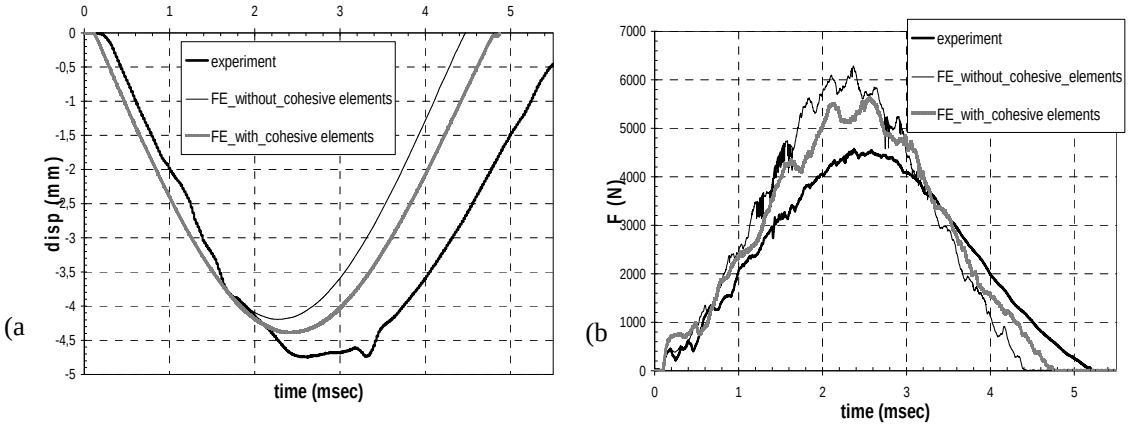

Figure 9: Comparisons of test and numerical rear face max deflections (a), impact forces (b) vs time

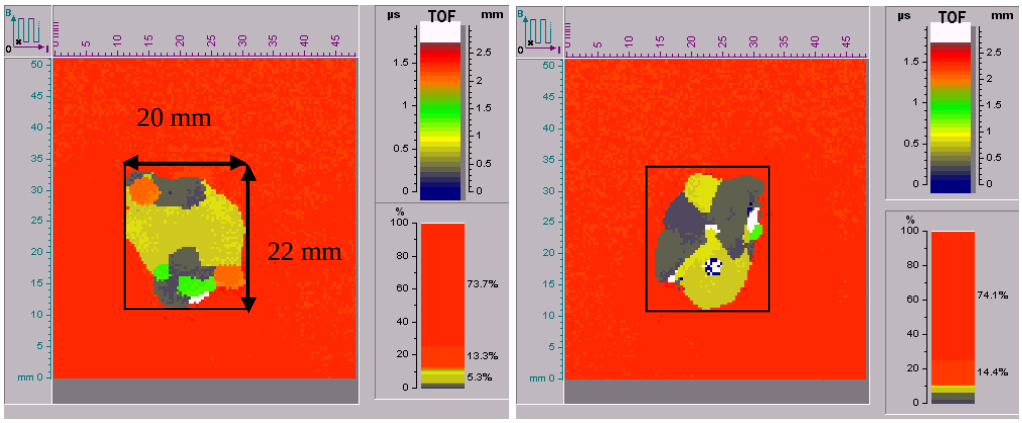

Figure 10: C-Scan pictures of the impacted plate (a) recto view from top, (b) verso view from bottom.

The total delaminated area in tests is about 20 mm × 22 mm (Figure 10). Corresponding numerical delaminated areas are delimited by elements which damage parameters are in [0.9;1[, which surround elements killed with damage equal to 1 as in the calibration phase (Figure 11 and Figure 12). Shapes and orientations of numerical delamination are consistent with the well known helicoidally through thickness repartitions: length along the lower ply orientation, and peanut shaped delaminations.

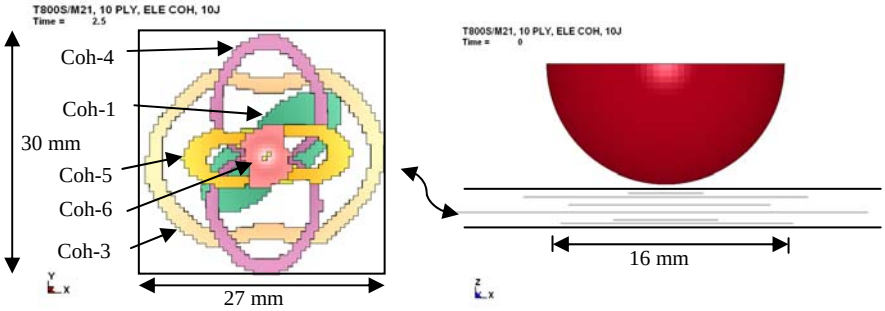

Figure 11: Delamination delimited by bands of elements which damage parameter is in [0.9; 1[at 2.5 ms.

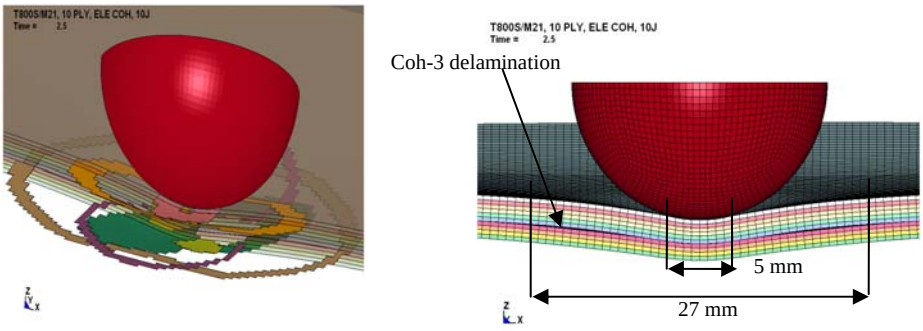

Figure 12: Delamination extension through the thickness at 2.5 ms.

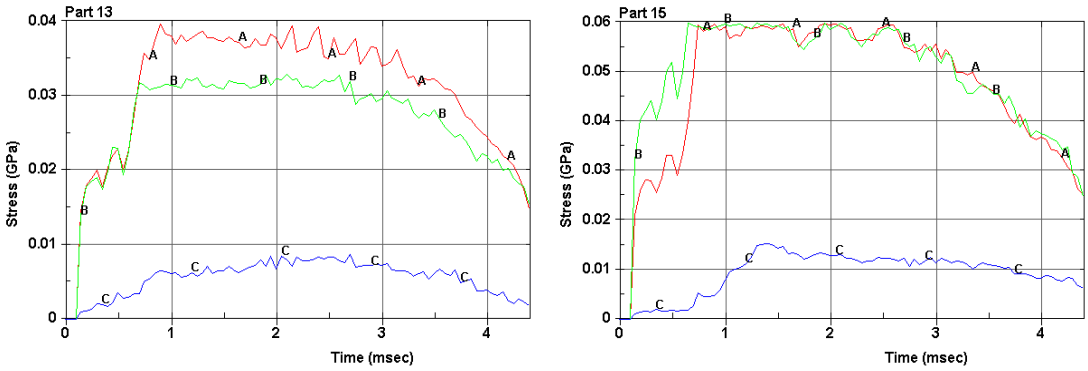

Figure 13: History of maximum tangential stresses (A & B) and normal stress (C) in [-45/45] coh-1 cohesive interface (LHS) and [90/0] coh-3 cohesive interface (RHS).

The diameter of contact area between the projectile and the plate has been measured in the simulations to be around 5 mm (Figure 12). This dimension is a typical length that can be measured in the center the coh-4, coh-5 and coh-6 delamination zones. As can be seen in Figure 11, cohesive elements have been killed or are almost fully damaged in those zones under the projectile, but the contact is closed between the adjacent layers. Thus, even if the total numerical delaminated area is higher than the experimental measure in the central [0/90] and [90/0] interfaces, they have dimensions similar to the experiment in the external interfaces (around 20mm length), and the physics of local punch and global bending is well reproduced. To this observation, we have plotted in Figure 13 curves of mode II and mode I maximum stresses in one “correctly” approximated interface, and a “less correctly” one. Tangential stress curves in both cases show a global round shape corresponding to the global bending of the plate, and local oscillations during the loading phase of the impact. These oscillations are related to the wave propagation and go back and forth in the thickness of the plate. In the coh-1 (bottom interface) where the delamination length is not consistent with the experiment, it is clear that the signal has not been truncated by the maximal tangential stress of 40 *MPa*, as is the case in the [90/0] coh-3 interface.

CONCLUSIONS

In this paper we have compared results of impact simulations using a developed bilinear cohesive model, with delamination and global force-displacement versus time curves, for a sample representative of composite material and layering typical of new aeronautical parts.

It has been shown that the computed delamination areas have the same shapes and dimensions in outer layers but are over estimated in the inner layers. This phenomenon is attributed to wave effects and loading rate effects that are not taken correctly into account by the existing model. As this point is crucial for higher velocity impacts, it will be the focus of further works especially for resin reach structures. A second point concerns the part of the stiffness loss due to delamination and due to through ply damage. Since the composite plies are assumed to be elastic, contact force is higher than and contact duration is lower than the experimental values. The incorporation of damage in plies will be the focus of future research.

ACKNOWLEDGEMENTS

The authors would like to acknowledge partial financial assistance from Higher Education Commission of Pakistan.

References

1. Elder D. J., Thomson R. S., Nguyen M. Q. and. Scott M. L., Review of delamination predictive methods for low speed impact of composite laminates. Composite Structures, 66:677–683, 2004.
2. Camanho P. P., Dávila C. G. and De Moura M. F., Numerical simulation of mixed-mode progressive delamination in composite materials. J. of Composite Materials, 37:1415–1438, 2003.
3. Iannucci L., Dynamic delamination modeling using interface elements. Computers and Structures, 84:1029–1048, 2006.
4. Pinho S. T., Iannucci L. and Robinson P, Formulation and implementation of decohesion elements in an explicit finite element code. Composites: Part A, 37:778–789, 2006.
5. Ilyas M., Limido J., Lachaud F., Espinosa Ch., Salaün M., Modélisation SPH 3D de l'impact basse vitesse sur plaque composite, Congrès Français de Mécanique, Marseille, 2009.
6. LS-Dyna Keyword User's Manual version 971, 2007, pp 535-538.
7. Ilyas M., Lachaud F., Espinosa Ch. Salaün M., Simulation of dynamic delamination and mode I energy dissipation, 7th European LS-DYNA Conference, Salzburg, 2009.
8. ISO 15024, Fibre-reinforced plastic composites—Determination mode I interlaminar fracture toughness, G_{Ic}, for unidirectionally reinforced materials, International Standard, © ISO 2001.
9. Maikuma H., Gillespie J. W. Jr., and Wilkins D. J, Mode II interlaminar fracture of the center notch flexural specimen under impact loading, Journal of composite materials, 24:124-149, 1990.
10. Prombut P., Caractérisation de la propagation de délaminage des stratifiés composites multidirectionnels, thèse de l'Université Paul Sabatier, ENSICA, DGM, 2007.